Journal of Membrane Science & Research

journal homepage: www.msrjournal.com

Research Paper

Electrochemical and Zeta Potential Effects of Monovalent Ions on Graphene-Zeolite PAN Composite Membranes

Salman Siddiqui [1], Mohammad Mujahid Ali Khan [2,*], Rafiuddin [1]

[1] *Membrane Research Laboratory, Department of chemistry, Aligarh Muslim University, Aligarh, India 202002.*
[2] *Applied Science and Humanities Section, University Polytechnic, Faculty of Engineering and Technology, Aligarh Muslim University, Aligarh, India 202002.*

Article info

Received 2025-04-04
Revised 2025-06-30
Accepted 2025-07-03
Available online 2025-07-03

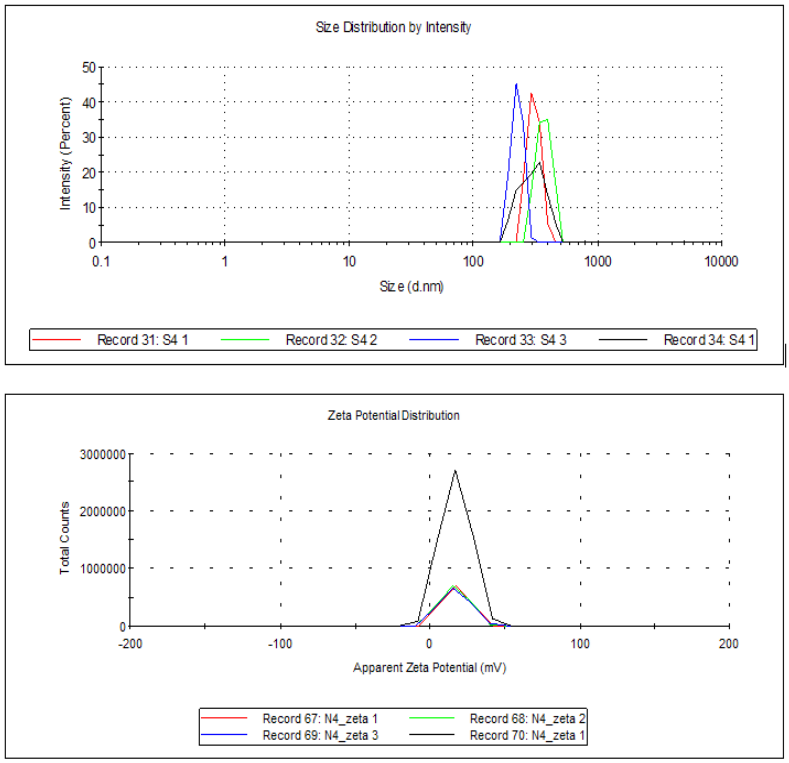
Keywords

Zeta potential
Conductivity
Electrochemical influence
Graphene powder
Perm selectivity
Polyacrylonitrile

Highlights

- Graphene-Zeolite PAN composite membranes
- Electrochemical influence of monovalent ions on the fabricated composite membranes.
- Electrochemistry of membrane in terms of Zeta potential and conductivity
- Fixed charge density calculated by Nagasawa, Kobatake, and Teorell Meyer Sievers.

Graphical abstract



Abstract

Electrochemically induced separations are primarily governed by membrane potential and ion perm selectivity. This study aimed to deepen the understanding of ion transport dynamics, electrical conductivity, and zeta potential in charged membranes. The measured membrane potential followed the trend: LiCl > NaCl > KCl > $NaNO_3$ > KNO_3, which correlates with variations in ion size, hydration energy, and mobility. To accurately assess fixed charge density, three well-established theoretical models Nagasawa, Kobatake, and Teorell-Meyer-Sievers were employed. Valuable electrochemical parameters, including membrane electrical potential, ionic transport number, and fixed charge density, were systematically analyzed to enhance membrane performance. Due to its strong electrostatic binding affinity with polymeric fixed charge groups, K^+ exhibited significantly lower perm selectivity compared to Li^+ and Na^+. Likewise, NO_3^- demonstrated reduced perm selectivity due to its larger hydrated ionic radius and lower charge density, which hinder its selective transport across the membrane. Higher the value of zeta potential show better stability. Ion exchange membrane's conductivity, selectivity, and electron transport characteristics are significantly influenced by swelling ratio, water uptake, IEC and porosity. Therefore, it as a promising candidate for large-scale industrial separation applications, particularly in water desalination, wastewater treatment, and chemical manufacturing.

© 2026 FIMTEC & MPRL. All rights reserved.

* Corresponding author: mujahidchemistry@gmail.com (M. M. A. Khan)

DOI: 10.22079/jmsr.2025.2057077.1714

1. Introduction

One of the top worldwide priorities is the rising need for clean freshwater to be consumed by people and ecosystems. Due to water shortage and lack of access to drinking water caused on by industrialization, population growth, and climate change, there are worries for people's health [1]. Industrial wastewater is a major contributor to the worldwide decline in freshwater resources because it contains dangerous and devastating wastes and chemicals, contaminants from waterborne diseases, heavy metal discharge, and agricultural waste. [2].

It is necessary to treat this effluent before releasing it into aquatic bodies. To deal with the worldwide water crisis and preserve and develop a sufficient supply of pure freshwater Scientists have been fascinated with membrane technology because of its very high salt rejection rate, lack of phase shift, simple operational control, low energy consumption, selective permeability, biocompatibility, and environmentally favourable features. [3].

Ion exchange membranes remain as one of most practical purification methods in this context and have applications in a number of areas, such as desalination of brackish and seawater, removal of hazardous metals from industrial effluents, the recovery of valuable ions, separation and purification of amino acids, and regulation of protein transport. They have also been used in development of pharmaceuticals and biotechnology products. Additionally, several studies have been conducted on the uses of these membranes in the chemical, food, and medical sectors. [4].

The membrane's stability and electrochemical performance are crucial for these applications. The selection of membrane materials and justification for picking materials stay crucial factors in the synthesis of a membrane that imparts total stability in all respects. Many different organic/polymeric materials, including PVC, PVA, PVDF, polystyrene, PAN and many more, have been extensively used as membrane materials. From these materials, a high degree of mechanical strength is shown by polyacrylonitrile (PAN), which has strong hydrogen bonds throughout its molecular structure. Additionally, it has high acid-proof alkalinity, strong chemical resistance, UV resistance, reduced sensitivity to humidity, and inexpensive cost. [5, 6]. In the last ten years, numerous researchers have been interested in it as a result. It is often used to make hollow fibre membranes, ultrafiltration membranes, and microfiltration membranes [7-9]. In addition to its characteristic, High absorption capacity, quick absorption speed, and outstanding dynamic performance are some of its distinctive characteristics. Some other characteristics of PAN are superior binding abilities, lipophilicity, affordability, and structural flexibility, PAN is a noteworthy polymer.

Despite having high membrane-forming abilities, outstanding physicochemical qualities, and great biocompatibility, polymeric membranes lack mechanical integrity, adsorption efficiency, irradiation resistance, and selectivity. This necessitates the insertion of inorganic fillers into organic matrix. By encouraging protonation-deprotonation, the addition of inorganic fillers not only lessens degree of plasticization of polymer but also strengthens it for improved transport qualities. These two materials' exceptional qualities are combined and their unique interfacial characteristics are synergistically improved by joining them into a single molecular composite. Electrostatic forces, van der Waals contacts, or weak hydrogen bonds all contribute to this interaction. [10-12].

Due to their thermal stability, selectivity for various metal ions, and preferred ion selectivity, zeolites-based composites are regarded as attractive alternatives for inorganic fillers. The inorganic filler and polymer binder qualities have a significant impact on the membrane's electrochemical performance and stability. [12]. Zeolites are coupled with other materials to synthesized binary, ternary, and other composites, which are referred to as zeolite-based composites. In general, zeolites are combined with carbon-based substances such as graphene metal oxides, polymers and clay compounds for a range of purposes, including fuel cells, catalysis, sorption, and ion-exchange membrane. Thus, when incorporating inorganic filler into a polymer matrix, it is important to take into account the aspect ratio and size of fillers. By selecting various ratios of both components and analysing their individual characteristics, attempts have been made to synthesise a membrane with appropriate chemical, thermal, and mechanical stabilities and exceptional transport qualities [13-22].

Understanding the electrochemical and transport characteristics is particularly crucial since they affect the composite membrane's effectiveness, selectivity, and permeability. Thus, the synthesis and electrochemical characteristics of composite (organic/inorganic) ion exchange membranes are described in this work [23-25].

In this study an inorganic filler (Fabrication of graphene on zeolites to from Zeolites-graphene (Z-GN) composite inorganic filler) was incorporated to PAN to obtained important parameters i.e. electrochemical properties, stability (chemical and Thermal), water content, porosity, swelling, thickness, and transport number etc. TMS model was used to evaluate the membrane's Charge density and membrane potential. Further, transport properties of membrane like transport number, Mobility ratio was also evaluated to study membrane performance and Conductivity of membrane was also examined by the four-probe method.

2. Experimental

2.1. Sonication of Graphene and zeolites

Graphene nanoplatelets (Gn, Alfa Aesar) and zeolites (Z) were individually subjected to ultrasonic dispersion using a high-frequency ultrasonic reactor (Labman) without any surface modification or functionalization. For each dispersion, 30 g of the material was suspended in a solvent mixture comprising 900 mL of deionized water and 100 mL of ethylene glycol, selected for its viscosity and ability to enhance cavitation efficiency. The sonication was performed for 30 minutes to achieve uniform particle dispersion and exfoliation. The process was carefully optimized under controlled physical parameters, including sonication temperature, pressure, and acoustic wave intensity, which significantly influence cavitation energy and, consequently, the dispersion quality. Post-sonication, the suspensions were filtered and the solids were dried at 200 °C to yield fine, uniform powders of graphene and zeolites. This method yielded highly exfoliated and well-dispersed graphene nanoplatelets, superior in purity and quality to those produced via conventional chemical methods such as Hummer's method. Unlike chemical oxidation-reduction processes, this physical route avoids introducing functional groups or structural defects, preserving the intrinsic properties of graphene. The ability to process both graphene and zeolites through sonication under controlled conditions enables scalable production of high-performance nanomaterials. These materials exhibit enhanced physicochemical properties, making them suitable for a wide range of applications in membrane science, catalysis, energy storage, and environmental remediation [26].

2.2. Synthesis of Gn-Z-PAN composite material and fabrication of membrane by hydrothermal process

Sonication plays a crucial role in the preparation of graphene–zeolite composites by enhancing dispersion and interfacial interaction between the two materials. The process uses high-frequency ultrasonic waves to break up agglomerates and promote uniform mixing, which is particularly important given the strong van der Waals forces that cause graphene sheets to stack and zeolite particles to clump together. Sonication also facilitates the exfoliation of graphene into few-layer or single-layer sheets, increasing its surface area and reactivity. This improved dispersion and exfoliation lead to stronger interactions between graphene and zeolite, ultimately enhancing the composite's properties, such as mechanical strength, thermal stability, adsorption capacity, or electrochemical performance, depending on the intended application

Sonicated Zeolites and graphene nanopowder in desired ratio were mixed together ultrasonically and dispersed in ethanol for 30 mins; then sonicated GN-Z were filtered and dried on 100ºC, obtained composite of Gn-Z was grind in mortar and pestle to ensure homogenous mixing of the Gn-Z to form and inorganic filler. In order to attain the necessary structural integrity, thermal stability, and mechanical stability of membrane, PAN sieved with mesh size of 200 (≥75 µm = 0.0029 inches) was utilised as a binder. In assembly of membrane, selecting right and appropriate quantity of binder are of utmost significance [27, 28].

The membrane made by embedding 25% PAN was appropriate; however, bigger amounts (>25%) and smaller amounts (5%) of PAN did not provide repeatable results and seemed unstable. As the polymer ratio increases, the proportion of barriers in the membrane increases; as a result, there are fewer cation exchange sites overall, which decreases electrochemical and transport characteristics of membrane and affects how it is applied. As the sonicated Gn-Z inorganic filler and Sieved 25% of PAN are stirred for 2 hours in 250ml solvent Dimethyl formamide (DMF), after 2 hours of stirring solution was kept in autoclave at 200ºC for 8-12 hours and sometime for a day. Heated solution is then cooled at room temperature, then it is filtered and obtained powdered is grind for 1 hrs for homogenous mixing of the composite. Powder was then pressed using a hydraulic press (SL-89, UK). The assembly of the membrane under 10 tonnes of pressure for 5-10 mins during fabrication. The membrane had been exposed in the proper electrolyte solution for at least a day before being used [29].

2.3. Gn-Z-PAN composite membrane surface morphology

The morphology and surface analysis were examined using a scanning electron microscope (JEOL JSM-65IO LV model), and energy dispersive X-

ray spectroscopy spectrum was analysed to confirm composition of synthesised nanocomposite membrane.

2.4. Gn-Z-PAN composite membrane TGA-DTA analysis

The thermogravimetric (TGA)/derivative weight (DTG) investigation entailed heating the polymeric nanocomposite sheets from room temperature to 800ºC at a rate of 20ºC per minute using a Shimadzu DTG-60 analyzer. Using the Van-Krevelan and Hofytzer equation, the limiting oxygen index (LOI) of the polymeric composite membrane was calculated from the Char yield portrayed in the TGA data. [30, 31].

$$LOI = 17.5 + 0.4 \times Char\ Yield \tag{1}$$

The integral procedural decomposition temperature technique (IPDT), which was initially proposed by Doyle (Zafar et al., 2020), was calculated using a TGA thermogram which is related to the flammable elements of the polymeric nanocomposite membrane.(Selim et al., 2018) This technique is used to assess the polymeric nanocomposite membrane's inherent heat resistance. IPDT may depict the complete curve's shape in a single Figure by computing the area under the curve. Using the formula below, IPDT was assessed in this research.

$$\mathrm{IPDT}(°\mathrm{C}) = \mathrm{A}^{*}\mathrm{K}^{*}\left(T_f - T_i\right) + T_i$$

$$A^{*} = \mathrm{Sl} + \frac{\mathrm{S2}}{\mathrm{Sl}} + \mathrm{S2} + \mathrm{S3}$$

$$\mathrm{K}^{*} = \mathrm{Sl} + \frac{\mathrm{S2}}{\mathrm{Sl}} \tag{2}$$

The surface area proportion for the full exploratory curve is A*, represented by the complete TGA thermogram, where Ti signifies the experiment's initially temperature and T_f marks its completion. The mathematical models of S1, S2, and S3 for finding A* and K* have been provided in a large number of published articles on IPDT [32, 33].

2.5. FT-IR and XRD analysis of Gn-Z-PAN composite membrane

Cu-K radiation (λ = 1.54 A), a scanning speed of 4 m/s, and a diffraction angle in range of 2=20-80ºC were used in an X-ray diffractometer (Rigaku Miniflex) examination to determine if the Nano-composite membrane is crystalline or amorphous. The d spacing and crystalline size is evaluated by Bragg's Eq. and the Debye-Scherrer Eq.

$$n\lambda = 2d\sin\theta$$

$$D = k\lambda / \beta\cos\theta \tag{3}$$

where D= Crystalline size (nm), k= Scherrer constant (0.94), λ= X-ray wavelength (1.54A), β= Line broadening at full width at half maxima [FWHM] in radian, θ= Bragg's angle in degree(º).

The Interspec 2020 FT-IR instrument was used to record the FT-IR spectra of the synthesised Nano-composite membrane at room temperature using Spectrolab (UK) KBr disc in order to determine the various functional groups and molecular composition.

2.6. Evaluation of the electrochemical studies and membrane stability of Gn-Z-PAN composite membrane

Study was conducted to assess the swelling ratio, ion exchange capacity (IEC), water uptake capacity and porosity and membrane potential measurements.

2.6.1. Swelling ratio (SR)

Swelling ratio is a parameter used to describe the membrane that is measured by comparing the thickness of the membranes when they are dry and after they have been equilibrated in different concentration of all the electrolytic solution for 24 hours. (Imteyaz and Rafiuddin, 2016b)

$$SR = \frac{A_{wet} - A_{dry}}{A_{dry}} \times 100 \tag{4}$$

where A_{Wet} and A_{Dry} represent the membrane's wet and dry areas respectively. Membranes were submerged in 1 M, 0.1 M, and 0.01 M salt solutions to determine the SR of membranes in each of the electrolytic salts employed. At the ambient temperature, the SR study was conducted. Structural qualities of polymers and their permeability to solutes are intimately connected to swelling characteristics of polymeric membranes [34-36].

2.6.2. Water Uptake

By observing the fluctuation in weight of membrane upon hydration, membrane's ability to absorb water was ascertained. Membranes were submerged in distilled water 2 two hours, and after water molecules had been washed from surface, membranes were weighed. The membrane was then weighed again to measure weight of dry membrane after having been in oven for 3 hours at 100 °C. Consequently, mass difference between dry and wet membranes was used to assess the membrane's capacity to absorb water:

Water uptake is being assessed by mass difference between the wet and dry membrane using the formula [37].

$$\text{water uptake}\% = \left(\frac{\mathrm{W_{wet}} - \mathrm{W_{dry}}}{\mathrm{W_{dry}}}\right) \times 100 \tag{5}$$

where W_{wet} and W_{dry} is weight of dry and wet membrane respectively.

2.6.3. Ion exchange capacity (IEC)

An acid-base titration technique was employed to measure ion exchange capacity. for 24 hours, membrane was kept submerged in a 0.1- M NaCl solution to facilitate cation exchange (H^+ with Na^+). Using phenolphthalein as the indicator, this solution, which contains substituted protons from membrane's phosphonic acid group, was titrated with 0.01-M NaOH; IEC value was obtained using the formula below:

$$IEC = \frac{N\,X\,V}{W}\, meq\, g^{-1} \tag{6}$$

where W is the weight measured in gm of the membrane and V and N are the volume and normality of the NaOH solution, accordingly. 0.1M HCl solution was used to replenish the membrane by converting it to the H^+ form for further usage.

2.6.4. Porosity

The amount of water that is residing within the membrane pores per unit volume was calculated to estimate porosity (ε) using the formula below.

$$\varepsilon = \left(\mathrm{W_w} - \mathrm{W_d}\right) / \rho_w \mathrm{AL} \tag{7}$$

where w represents the water's density, A and L stand for the membrane's area and thickness, accordingly, W_w and W_d for the membranes' respective masses.

2.6.5. Evaluation of Electrochemical parameters of Gn-Z-PAN composite membrane

Individual membranes (effective area of 4.71 cm2) remained positioned across the two separate sections of a glass container in an upright position. Electrolyte solutions (nitrates and chlorides of Na^+ and K^+) in each section have an overall capacity of 30 ml and ranged in concentration between 0.01 M to 1 M; five various concentrations were employed to ensure a 10-fold difference. Nitrates and chlorides, two of most frequent ions in tap water, are toxic to people's health. Fig. 1 shows an electrochemical setup designed for measuring membrane potential. Prior to analysis, solutions were stirred with a magnetic stirrer to limit the effects of concentration polarisation and avoid formation of a boundary layer at membrane's surface. The potential difference between the different membranes was calculated using a digital potentiometer (Electronics India 118). A saturated calomel electrode served as the working electrode, while a silver chloride electrode served as reference electrode.

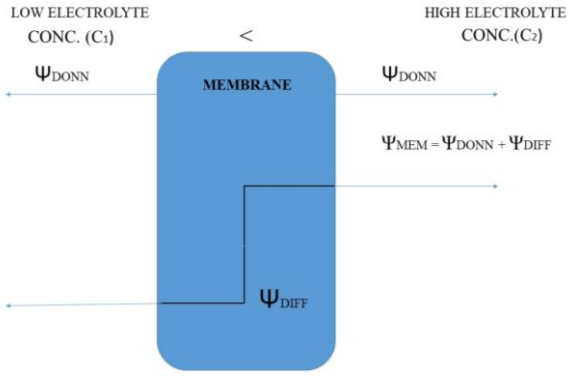


Fig. 1. Membrane potential electrochemical setup.

Membrane potential, transport number, mobility ratio, charge density, and permselectivity were explored as electrochemical parameters. Taylor-Mayor and Sievers equation (TMS) was used to evaluate the various parameters like Fixed charged density, Mobility ratio, transport number and permselecitivty.

2.6.5.1. Taylor-Mayor and Sievers Theory

Taylor-Mayor and Sievers (TMS) has every solution- membrane interface has a state of equilibrium process that is formal analogous to the Donnan equilibrium.

(a) All through the membrane's phase, cation and anion mobilities, fixed charge concentration, (b) Transferred state of water may be disregarded, are all constant as well as independent of salt concentration. These hypotheses' ramifications have been examined. Another presumption is the notion that activity coefficient of the salt is identical at each interaction in the membrane and solution phases. merely the Donnan potential, utilising either integration of the Planck or Henderson equations, can rectify the introduction of concentration-related activities. [38].

As per the TMS theory membrane potential at 25°c is given by

$$\Delta\emptyset = 59.2\left(log\frac{c_2}{c_1}\frac{\sqrt{4C_1{}^2+D^2}+\bar{D}}{\sqrt{4C_2{}^2+\bar{D}^2}+\bar{D}}+\bar{U}log\frac{\sqrt{4C_2{}^2+D^2}+\bar{D}\bar{U}}{\sqrt{4C_1^2+D^2}+DU}\right) \quad (8)$$

$$U=\frac{\bar{u}-\bar{v}}{\bar{u}+\bar{v}} \quad (9)$$

where, in membrane phase, u and v, denote cation and anion mobilities ($m^2v^{-1}s^{-1}$). Concertation of the solution is represented by C_1 and C_2, and charge density of membrane is shown by D as equivalents per unit volume.

2.7. Conductivity and Zeta potential

The ability of a component to act as a conductor of electric current is determined by its level of electric conductivity. The movable charge of an electrical potential item will move and produce an electric current if it is positioned at the ends of a conductor. Electric conductivity is measured by four probes with the help of digital microvoltmeter (DMV-001) and constant current source (CCS-01). Whereas zeta potential was determined by the (Nano-ZS Zetasizer, Malvern instruments) with back scatter detection.

3. Results and discussion

3.1. Surface morphology of Gn-Z-PAN composite membrane

Surface determination of Gn-Z-PAN composite membrane was done by the SEM as shown in Fig. 2. SEM evaluation was done to investigate morphological change on surface after loading of PAN on Gn-Z.

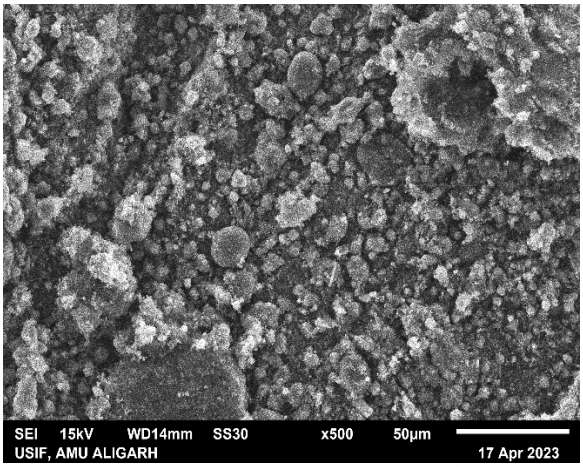


Fig. 2. SEM image of Gn-Z-PAN composite membrane.

Fig. 2 demonstrates the smooth planar morphology of the inorganic component, which, when combined with polymer, exhibits intergranular cavitation and a porous structure with a loose array of grains and micro voids and no surface aggregation. This proves that the composite membrane is permeable.

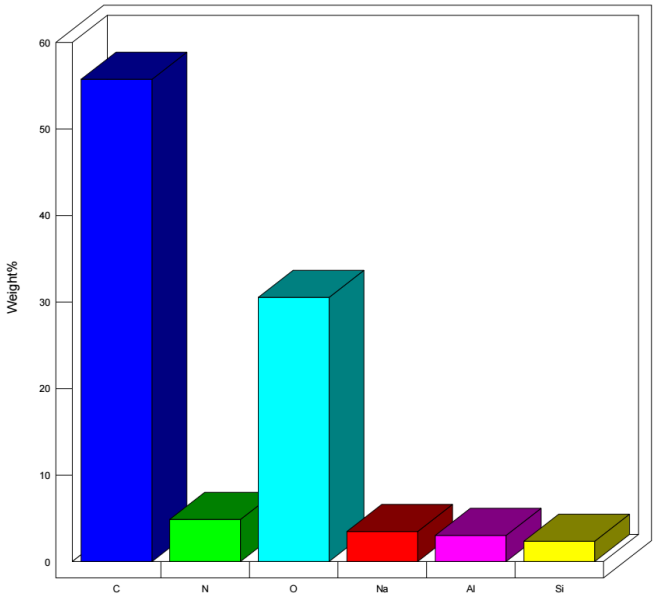


Fig. 3. EDX spectrum of Gn-Z-PAN composite membrane.

Fig. 3 EDX of Gn-Z-PAN depict presence of Carbon (C), Nitrogen (N), Oxygen (O), Sodium (Na), Aluminium (Al), Silicon (Si) shows that the membrane is synthesised in the proper way and is ready for the further use.

3.2. TGA-DTA analysis of Gn-Z-PAN composite membrane

Fig. 4 depict the TGA spectrum of nanocomposite synthesised membrane i.e. Gn-Z-PAN. TGA spectrum depict a breakdown at 120 °C which is due the moisture presents in synthesised membrane. Slight weight of 2.87% of solid materials is responsible for Degradation between 300°C-450°C. and the weight loss of 12.23% at degradation of Gn-Z-PAN and breakdown of unstable oxygen group present in the synthesized membrane is in between 480°C-780°C [38]. The DTA spectrum of synthesised membrane which show the obvious exothermic peak at 380°C.

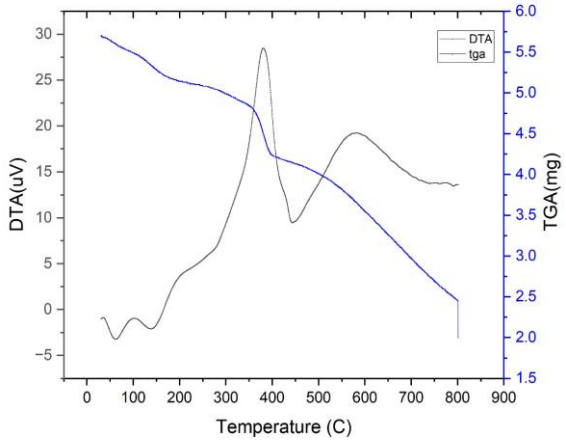


Fig. 4. TGA-DTA curve of Gn-Z-PAN composite membrane.

3.2.1. Flame retardant behaviour of Gn-Z-PAN composite membrane

At 800°C with TGA, Flame resistance of polymer and synthesised membrane as shown in the Table 1. The LOI value may be employed to get an exact estimate of the likelihood that these polymers will be employed in flame-resistant applications. It is going to ignite slowly in the air if the polymer's LOI falls below than 20.9, sluggish burning between 21 and 28, self-extinguishing behaviour between 28 and 100, burn slowly between 100 and higher than 100, and not burn at all if the LOI is larger than 100 [39].

3.3. FTIR and XRD spectrum of Gn-Z-PAN composite membrane

3.3.1. FTIR spectrum of Gn-Z-PAN composite membrane

FTIR spectrum of Gn-Z-PAN nanocomposite was depicted in Fig. 5. Which have the following peak. Peak at 552 cm^{-1} is due to Si-O stretching vibrations and the peak at 1080 cm^{-1} is due to the bending vibration of the Si-O-Si bond indicate the presence of Zeolites. The peak at 1579 cm^{-1} corresponds to C-N vibration and Peak around 1635 cm^{-1} is due to C=C vibration shows the presence of the Poly-acrylonitrile in the synthesized membrane. The peak around 2960 cm^{-1} is due to CH_2 vibration and peak around 3393 cm^{-1} is due to OH vibration attributes for graphene Nano-powder [40-44].

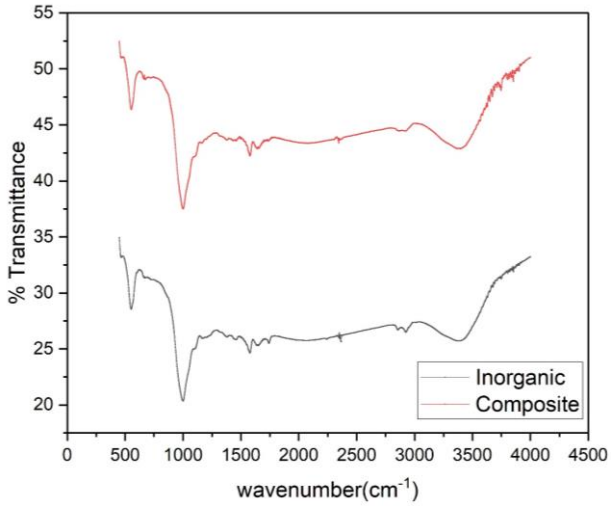


Fig. 5. FTIR spectrum of Gn-Z-PAN composite membrane.

3.3.2. XRD spectrum of Gn-Z-PAN composite membrane

XRD spectrum of Gn-Z-PAN nanocomposite was depicted in Fig. 6. Gn-Z-PAN nanocomposite main diffraction peak at 2θ levels shown in the Table 1, Diffraction peak at 7.27, 10.2,12.5,30.3 and 32.6 attributed for the zeolites, whereas diffraction peaks at 21.7, 24.3 indicated the presence of graphene (AlShammari et al., 2019) and the limited peaks at 16.2 and 20.5 indicated the PAN which is presented in the crystalline synthesised nanocomposite [45, 46].

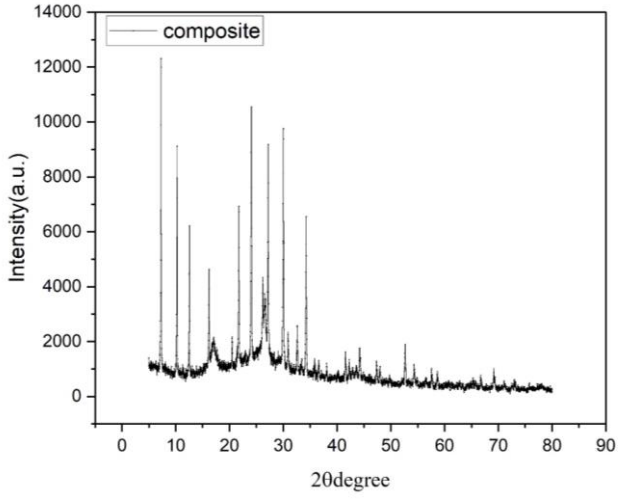


Fig. 6. XRD spectrum of Gn-Z-PAN nanocomposite membrane.

Table 1
XRD parameters of Gn-Z-PAN composite membrane 2θ, D spacing, crystalline size and FWHM.

Degree	D spacing (nm)	Crystallite size	FWHM β (°)
7.27	12.15	780	.08978
10.2	8.6	782	.09256
12.5	7.05	784	.09103
16.2	5.4	787	.13752
20.5	4.3	791	.15111
21.7	4.05	543	.15022
24.3	3.65	545	.15000
27.3	3.2	908	.1690
30.3	2.9	633	.16279
32.6	2.74	556	.15756
52.8	1.73	595	.14987
		700.36 Avg size	

The average crystalline size i.e. 700.36 of the nanocomposites has been computed by Debye-Scherrer equation using X'Pert High Score Plus V3.0

$$D = \frac{K\lambda}{\lambda COS\theta} \tag{10}$$

K is Scherrer's constant (K = 0.94), λ denote wavelength of X-ray radiation, λ stand for full width at half maximum (FWHM) and θ is diffraction angle.

3.4. Electrochemical evaluation and membrane stability parameters of fabricated graphene powder and zeolite-loaded PAN composite membranes

The characteristics of the membranes are significantly impacted by the amount of water in the membrane. Ion exchange membrane's conductivity, selectivity, and electron transport characteristics are significantly influenced by swelling ratio, water uptake, IEC and porosity.

Synthesized Gn-Z-PAN composite swelling ratio, water uptake, IEC and porosity was respectively found to be 8, 12.85, 0.685, 0.267. It has been additionally discovered that the porosity of ion-exchange membranes affects both ion selectivity and transport. Pores larger compared with an ionic species cannot accommodate that species. Although membranes with greater porosities will limit ion selectivity, they also serve as non-conducting regions for ionic species [47].

3.4.1. Membrane Potential of zeolite loaded PAN composite membranes

Water absorption and porosity have a significant impact on the ion exchange membrane's membrane potential. As more water is integrated into the matrix, increased protonic mobility is produced, which is supported by water passageways, and significant values of swelling ratio, IEC, and porosity result in favourable membrane potentials [48, 49].

Membranes frequently react to small gradients which are present on the opposite side of the membrane. The dialysis procedure was carried out using the concentration gradient. A charged membrane forms a contact zone throughout the membrane while in contact alongside an identical electrolytic salt that has different concentrations. Due to uneven movement of ions caused by different concentration of electrolytes, a potential difference between two contributions of Donnan and a diffusion potential occurs [36, 49].

Fig. 7a depict potential values of the Gn-Z-PAN composite membrane were plotted against -log C_2 in for varied concentrations of Licl, NaCl, KCl, $NaNO_3$, and KNO_3 salts. The composite membrane's cation selectivity is confirmed by the membrane potential, which becomes positive as the electrolyte concentrations drop. This is due to structural modifications made to electrical double layer at solution membrane interface. Electrolytic ions' varied sizes are represented by potential values in following order: LiCl>NaCl > KCl > $NaNO_3$ > KNO_3. The smaller cation size resulted in a rise in membrane potential (Table 2).

Variations in anions are observed based on their size, mobility ratio, and robust contact with membrane matrix. Membrane potential is greater for Cl, which has a smaller size and better mobility, than for NO_3, which has a larger size and stronger relationship to the membrane matrix. Charges found on pore walls of membrane will reject both Cl^- and NO_3^- co-ions [50].

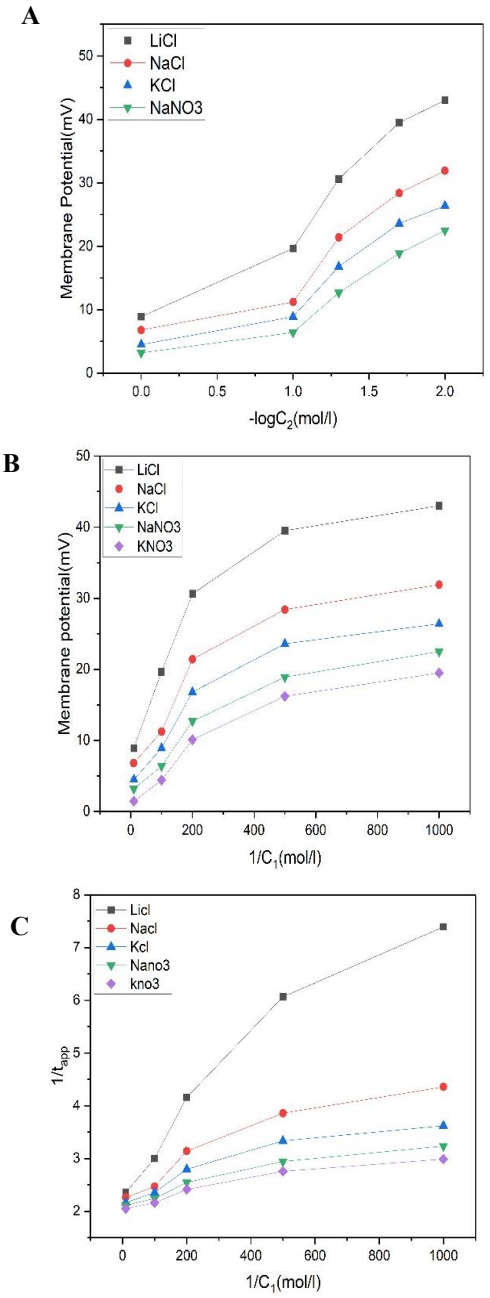


Fig. 7. (a) Observed membrane potential φ_m vs. log C_2, (b) Observed membrane potential vs.$1/C_1$ and (c) inverse of transport number vs. $1/C_1$ for different electrolytes across Gn-Z-PAN composite membrane.

Table 2
Potential at different electrolytic concentration of Gn-Z-PAN composite membrane.

Electrolyte conc C2/C1 (mol/l)	LiCl	NaCl	KCl	$NaNO_3$	KNO_3
1/0.1	8.9	6.8	4.5	3.2	1.45
0.1/0.01	19.65	11.2	8.9	6.4	4.4
0.05/0.005	30.6	21.4	16.8	12.7	10.1
0.02/0.002	39.5	28.4	23.6	18.9	16.2
0.01/0.001	43	31.9	26.4	22.5	19.5

The membrane potential is dependent on ion diffusion, therefore Cl^-(small size) would propagate more quickly, leaving NO_3^- (big size) behind, which would have a longer period to repel and get attracted to opposing charge existing on membrane wall.

3.4.2 Transport number and mobility ratio of Gn-Z-PAN composite membrane

The transport number is proportion of the total current that opposing ions carry through the membrane. Membrane potential, that may be evaluated to determine transport number and is provided by following equation, occurs when membrane is separated by uneven electrolyte solutions.

$$\Psi_m = \frac{RT}{F}\left(t_+ - t_-\right) ln \frac{C_2}{C_1} \tag{11}$$

where R, T, and F stand for Faraday constant, gas constant, and absolute temperature, correspondingly. Electrolyte solution concentrations in the testing glass chamber are C_1 and C_2. Membrane's distinctive electrical charge affects transport property and mobility ratio as in Fig. 8 a & b. Ion transport is impacted by membrane's effective charge. Due to various mobilities of co-ions and counter-ions in membrane, Donnan effect of co-ions may be disregarded for membranes that are just weakly charged. The membrane potential is primarily determined by the diffusion potential, and its expression(Klaysom et al., 2010) [23, 24, 51]. (for 1: 1 electrolytes) is

$$U = \left| \frac{t_+}{|Z_+|} - \frac{t_-}{|Z_-|} \right| \tag{12}$$

$$\bar{\omega} = \frac{\overline{U}}{V} = \frac{t_+}{t_-} \tag{13}$$

Here, Z+ and Z- stand in for cation and anion valences, U is a quantity related to the aggregate transport numbers of ions in membrane, t+ and t- stand for cation and anion transport numbers, and u as well as v are, respectively, their molar mobilities. Mobility ratio ($\bar{\omega}$) is the proportion of molar mobilities of cation to anion. In this research, the composite membrane's transport number at lower Li salt concentrations went up to 0.86 as shown in Fig. 8b and Table 3, showing a minor deviance from ideal ion-selective characteristic of 1.00 [52, 53].

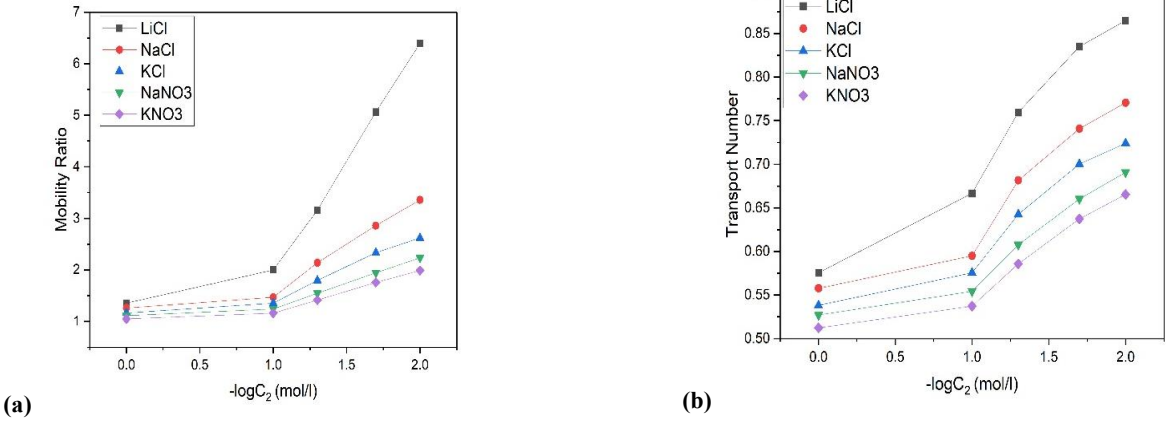


Fig. 8. (a & b) Mobility ratio and transport number of Gn-Z-PAN composite membrane respectively.

Table 3
Transport number and mobility ratio of Gn-Z-PAN composite membrane.

Electrolyte Conc	LiCl		KCl		$NaNO_3$		KNO_3	
	t+	ω	t+	t+	ω	t+	t+	ω
1	0.5755	1.35569	0.55768	0.55768	1.35569	0.55768	0.55768	1.35569
0.1	0.66668	2.00015	0.59501	0.59501	2.00015	0.59501	0.59501	2.00015
0.05	0.75957	3.15919	0.68153	0.68153	3.15919	0.68153	0.68153	3.15919
02	0.83506	5.06295	0.74091	0.74091	5.06295	0.74091	0.74091	5.06295
0.001	0.86475	6.39388	0.7706	0.7706	6.39388	0.7706	0.7706	6.39388

Assuming that transport number is constant across membrane, it is also possible to calculate counter-ion transport number in membrane phase for different 1: 1 ions using membrane potential ψ_m. However, it is possible to estimate transport number of counter-ions inside membrane phase more precisely when effective concentration of the membrane's ion-exchange site is much lower than the electrolyte concentration. Previous studies have shown a correlation between electrolyte concentrations and membrane potential.

$$\varphi_m = \frac{RT}{F}\left(2t_+^m - 1\right)ln\gamma + \frac{2(\gamma-1)}{\gamma}\left(1-t_+^m\right)t_+^m\frac{\theta X}{C_1} \tag{14}$$

Thus, the terms "t^+_m" and "X" represent as counter-ion transport number and "% of fixed charge in the membrane phase," accordingly. You may evaluate the fixed charge density in membrane phase and t_+^m based on intercept and slope values by plotting graph of m against 1/C1. In order of increasing t_+^m number, NaCl, KCl, NaHCO3, and $KHCO_3$ are present. Table 4 shows that membrane becomes more selective towards the Li^+ ion since selectivity is inversely associated with the quantity of counter ions that are carried. Table 5 lists the values for both parameters [54, 55].

Table 4
Evaluated parameters of t_+^m, X, α and β Gn-Z-PAN composite membrane.

Electrolyte	LiCl	NaCl	KCl	$NaNO_3$	KNO_3
α	.5934	.5923	.5681	.5475	.5305
β	4.428	3.701	2.972	2.421	1.733
θX	1.13×10^{-2}	$.477\times10^{-2}$	$.306\times10^{-2}$	$.253\times10^{-2}$	$.213\times10^{-2}$
t_+^m	.6468	.5950	.5719	.5503	.5332

3.5 Different theoretical models' assessments and comparisons of fixed charge densities

3.5.1 Nagasawa

Equation was provided by Nagasawa et al.

$$-\varphi_m = \frac{RT}{F}\left(\frac{\gamma}{\gamma-1}\right)\left(\frac{\theta X}{2}\right)\frac{1}{C_1} \tag{15}$$

To determine membrane's fixed charge density. When isolated by electrolyte concentrations C1 and C2 that are not identical, where X is the membrane's constant charge density and γ= 10. The membrane potential is depicted in Fig. 7b as a function of electrolyte concentration. In the examined concentration range, the membrane exhibited straight lines. This shows that the electrolyte concentrations and membrane potential are negatively correlated. Fixed charge density of composite membrane may also be determined using slope values (Table 5) [56].

Table 5
Fixed charge density evaluated value using various theoretical model of Gn-Z-PAN composite membrane.

Electrolyte	LiCl	NaCl	KCl	$NaNO_3$	KNO_3
TMS	$.599\times10^{-2}$	$.887\times10^{-2}$	$.998\times10^{-2}$	1.11×10^{-2}	1.27×10^{-2}
Nagasawa	$.0155\times10^{-2}$	$.0165\times10^{-2}$	$.0181\times10^{-2}$	$.020\times10^{-2}$	$.0265\times10^{-2}$
Kobatake Low	1.012×10^{-2}	1.02×10^{-2}	1.027×10^{-2}	1.031×10^{-2}	1.036×10^{-2}
Kobatake High	$.0521\times10^{-2}$	$.539\times10^{-2}$	$.601\times10^{-2}$	$.712\times10^{-2}$	$.795\times10^{-2}$

3.5.2. Kobatake

Kobatake offers a model for membrane potential that is appropriate for charged membrane isolated by electrolyte solutions of varying concentrations, which starts with fundamental flow formula based off thermodynamics of irreversible processes. Two limiting versions are available [53].

1. Fixed charge density of composite membrane may be estimated as follows when C1 is appropriately modest with a fixed γ (10) value:

$$\varphi_m = \frac{RT}{F}\left(\frac{1}{\beta}ln\gamma - \left(\frac{\gamma-1}{\alpha\beta\gamma}\right)\left(1+\frac{1}{\beta}-2\alpha\right)\frac{C_1}{\theta X}\right) \tag{16}$$

where relates to a selectivity of ions on the membrane and relates to the impact of ion adsorption on the membrane material. The fixed charge density may therefore be calculated by plotting m against C1, with the intercept and slope are, respectively, β and α.

2. Utilising membrane potential measurements and the $t_{_app}$ from equation, fixed charge density at high concentrations of salt with fixed γ (10) value may be further evaluated:

$$\varphi_m = \frac{RT}{F}\left(1-2t_app\right)ln\frac{C_2}{C_1} \tag{17}$$

where in the correlation of the apparent transport number to the concentration is inverse for co-ion species in a negatively charged membrane. Nernst form of equation may be used to compute the apparent transport number.

$$\frac{1}{t_app} = \frac{1}{1-\alpha} + \frac{\alpha(\gamma-1)}{(1-\gamma)\gamma - ln\gamma}\left(\frac{\theta X}{C_1}\right) \tag{18}$$

Inverse of apparent transport number plot in Fig. 7c provides value of fixed charge density of membrane from value of intercept using Eqs. (16) and (17). Table 5 provides the values of and as determined above.

By an TMS equation, a fixed charge density has been calculated using theoretical observations of membrane potential. The quantity D in the TMS equation stands for the charge density, which is connected to the membrane's necessity for electro neutrality. A series of both theoretical and experimental potential curves have been plotted against -log C2 taking into account a membrane with different charge densities D1 for a 1:1 electrolyte solution, as illustrated in Fig. 9. The experimental curve's coincident point provided the real fixed charge density D of membrane phase [57].

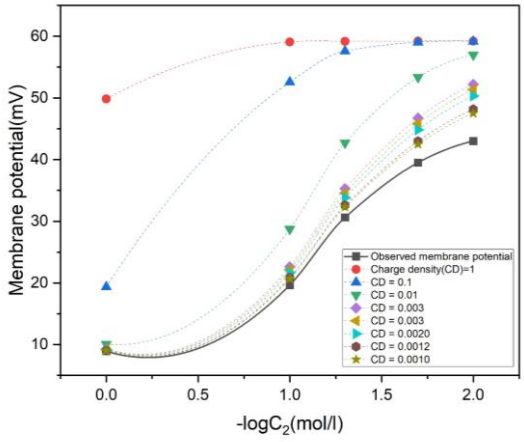


Fig. 9. Membrane potential ψ_m Vs. -log C_2 for Gn-Z-PAN composite membrane using TMS. With a constant D = 1 value and a varied mobility ratio, each smooth curve represents theoretical membrane potentials.

The ratio of –log x, which was computed and denotes value of fixed charge density, was found in Fig. 11 at the intersection of the theoretical and experimental membrane potential curves for each electrolyte. Since bigger ions have stronger ionic atmospheres, trend in fixed charge density for electrolyte solutions were contrary to that of membrane potentials, namely LiCl>NaCl > KCl > $NaHCO_3$ > $KHCO_3$.

3.6 Perm selectivity of Gn-Z-PAN composite membrane

It is believed that a cation-exchange membrane is entirely permselective. If only counter ions can pass through while co-ions are blocked. Co-ion transport may result from field-driven migration of co-ions or diffusive (concentration-driven) transport of co-ions from a high concentration to a low concentration, with the relative magnitude of each form of transport depending on the concentration difference and the strength of the applied electric field. Transport number may be used to compute the permselectivity (Ps) for a cation exchange membrane using the Eq.

$$P_s = \frac{\left(t_+^m - t_+\right)}{t_-} \tag{19}$$

where in the values of t_+^m and t_+ stand for transport numbers of counter- and co-ions in solution phase, respectively, and t is transport number of counter-ions in the membrane phase [58, 59].

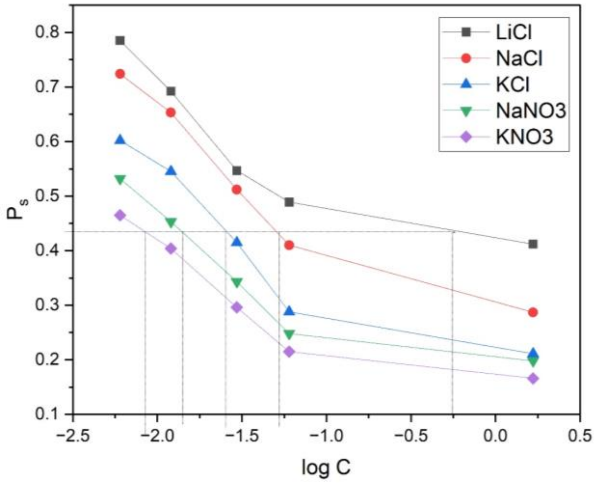


Fig. 10. Gn-Z-PAN composite membrane, plots of Ps Vs log C for different monovalent electrolytes.

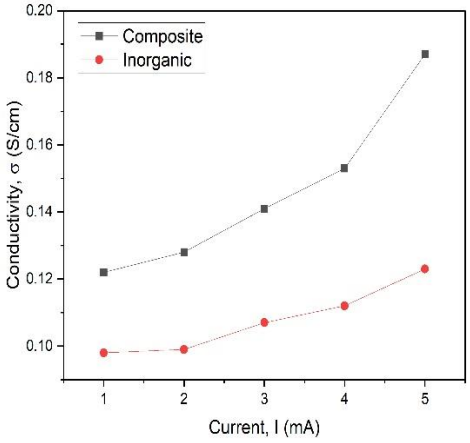
Perm selectivity depends on membrane variable rather than the kind of counter-ions and co-ions or volume of solutions. As the concentration of bulk phase increases, Fig. 10 shows that an increase in counter- and co-ion content in membrane phase results in a decrease in the perm selectivity. Consistent values demonstrate that this causes a reduction in the perm selectivity and an increase in their electrostatic attraction to one another. Fixed ionic group and opposing ions might be the culprits in this. Na+ and K+ have smaller hydrated radii than Li+. Since each of these cations has a constant electric charge, an ion's mobility ratio and permanent selectivity become worse as it gets bigger [58, 59].

3.7. Conductivity and Zeta potential of Gn-Z-PAN composite membrane

Conductivity of Gn-Z-PAN composite membrane is evaluated by the ohm's law,

$$V = IR \tag{20}$$

where V is the voltage applied across the conductor, I is the current flowing through it, and R is the resistance the conductor imposes on the current flow.



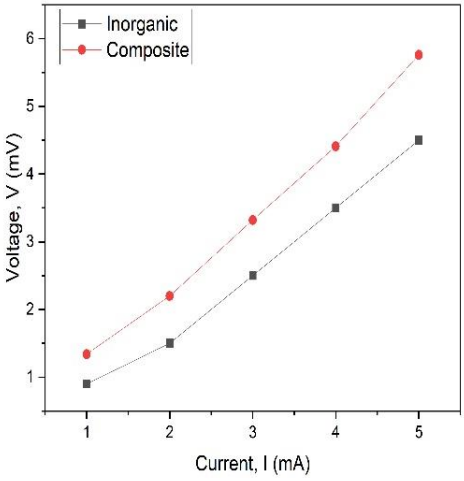


Fig. 11. Gn-Z-PAN composite membrane plot of Conductivity Vs I and Voltage Vs I.

As shown in Fig. 11 both plot of conductivity vs I and voltage Vs I flow the ohmic law and synthesized membrane is conductive in nature.

Zeta potential is a crucial metric because it shows how well they can transport contrast materials for ultrasonic imaging, which must be innocuous and simple to find and remove during in-vivo use. It is generally recognised that a larger absolute value of zeta potential indicates a more stable state for colloidal systems, and potential levels higher or lower than +30 mV allow for a suspension that is essentially stable.

Fig. 12 it is clearly depicted that average size of the synthesized membrane is 552 nm and the zeta potential value of 17 which depicted that the synthesised membrane is incipient stability (higher value of zeta potential negative or positive show better stability) and suitable for further usage.

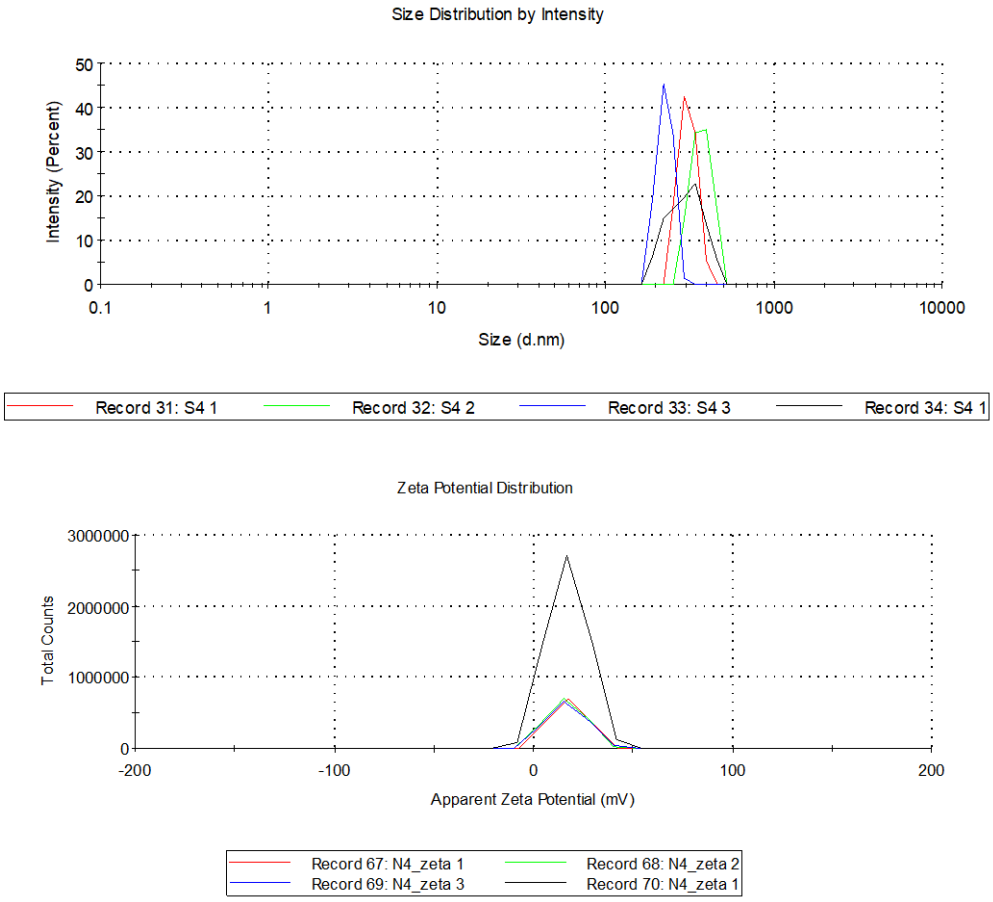


Fig.12. Average size and zeta potential value of Gn-Z-PAN composite membrane.

4. Conclusions

A novel cation exchange membrane (Gn-Z-PAN) was fabricated by hydrothermally incorporating a graphene–zeolite (Gn-Z) inorganic composite into a polyacrylonitrile (PAN) matrix. FT-IR spectra confirmed strong intermolecular interactions between PAN and Gn-Z, while XRD analysis indicated crystalline structure with an average crystallite size of 700.36 nm. TG-DTA analysis demonstrated good thermal stability, and SEM images revealed a porous surface morphology.

Stability studies identified 25% PAN content as optimal, offering a balance between mechanical strength from polymer cross-linking and thermal stability from the inorganic filler. Membrane potential measurements using monovalent electrolytes (LiCl, NaCl, KCl, $NaNO_3$, KNO_3) followed the trend: LiCl > NaCl > KCl > $NaNO_3$ > KNO_3, indicating higher membrane potentials for smaller cations due to enhanced mobility and stronger Donnan exclusion. Cl^- ions showed greater mobility and interaction with the membrane than NO_3^-, resulting in higher potentials. As electrolyte concentration increased, membrane potential decreased, confirming its cation-selective behaviour and Ohmic conductivity. Fixed charge density, calculated using models like Nagasawa, Kobatake, and TMS, showed good agreement with experimental data, with Li^+ exhibiting the highest fixed charge due to its exclusion from the membrane matrix. Perm selectivity was highest for LiCl and lowest for KNO_3, with reduced selectivity for K^+ due to its strong interaction with fixed charges, which lowers charge density. The membrane showed good conductivity, with an average particle size of 552 nm and a zeta potential of +17 mV, confirming its suitability for electro-membrane applications such as selective ion separation and energy devices.

Acknowledgements

Salman Siddiqui is grateful to the Chairman, Department of the Chemistry of Aligarh Muslim University, Aligarh, for providing research facilities. We appreciate the Departmental Instrumentation facilities to support XRD and FT-IR. We also appreciate the SEM and TEM facilities at the University Sophisticated Instrumentations Facility (USIF), AMU. In addition, acknowledge University Grants Commission (UGC), New Delhi, for financial support.

Authors contribution

Salman Siddiqui (MSc) and Mohammad Mujahid Ali Khan (PhD) designed the study, Conceptualization, Experimental design, Data analysis, Writings-review and manuscript editing. **Rafiuddin (Prof):** Supervision, Visualization, Formal analysis.

Data availability

The data supporting this study's findings will be made available from the corresponding author upon reasonable request.

Declaration of Interest Statement

All authors contributed to the study conception and design. Material preparation, data collection and analysis were performed by [Salman Siddiqui] and [Mohammad Mujahid Ali Khan] and supervise by [Rafiuddin]. All authors read and approved the final manuscript.

CRedit authorship contribution statement

M. M. A. khan: Lead
S. Siddique: Equal
Rafiuddin: Supervisor

References

[1] Lee, W.W., Lu, C.-S., Chuang, C.-W., Chen, Y.-J., Fu, J.-Y., Siao, C.-W., Chen, C.-C., 2015. Synthesis of bismuth oxyiodides and their composites: characterization, photocatalytic activity, and degradation mechanisms. RSC Adv. 5, 23450–23463. https://doi.org/10.1039/C4RA15072D.

[2] Pendergast, M.M., Hoek, E.M.V., 2011. A review of water treatment membrane nanotechnologies. Energy Environ. Sci. 4, 1946. https://doi.org/10.1039/c0ee00541j

[3] Razali, M., Kim, J.F., Attfield, M., Budd, P.M., Drioli, E., Lee, Y.M., Szekely, G., 2015. Sustainable wastewater treatment and recycling in

membrane manufacturing. Green Chem. 17, 5196–5205. https://doi.org/10.1039/C5GC01937K.
[4] Khan, M. M. A., & Rafiuddin. (2011). Synthesis, characterization and electrochemical study of calcium phosphate ion-exchange membrane. Desalination, 272(1–3). https://doi.org/10.1016/j.desal.2011.01.041
[5] Chang, Z.J., Zhao, X., Zhang, Q.H., Chen, D.J., 2010. Nanofibre-assisted alignment of carbon nanotubes in macroscopic polymer matrix via a scaffold-based method. Express Polym. Lett. 4, 47–53. https://doi.org/10.3144/expresspolymlett.2010.8.
[6] Heikkila, P., Harlin, A., 2009. Electrospinning of polyacrylonitrile (PAN) solution: Effect of conductive additive and filler on the process. Express Polym. Lett. 3, 437–445. https://doi.org/10.3144/expresspolymlett.2009.53.
[7] Li, S.-F., Chen, J.-P., Wu, W.-T., 2007. Electrospun polyacrylonitrile nanofibrous membranes for lipase immobilization. J. Mol. Catal. B Enzym. 47, 117–124. https://doi.org/10.1016/j.molcatb.2007.04.010
[8] Wang, T., Kumar, S., 2006. Electrospinning of polyacrylonitrile nanofibers. J. Appl. Polym. Sci. 102, 1023–1029. https://doi.org/10.1002/app.24123
[9] Yoon, K., Kim, K., Wang, X., Fang, D., Hsiao, B.S., Chu, B., 2006. High flux ultrafiltration membranes based on electrospun nanofibrous PAN scaffolds and chitosan coating. Polymer (Guildf). 47, 2434–2441. https://doi.org/10.1016/j.polymer.2006.01.042
[10] Nyiko M. Chauke, Tshimangadzo S. Munonde, Nomvano Mketo , (2025) A critical review of the anti-biofouling properties of biogenic-based silver nanoparticles (AgNPs) embedded on polymer membranes for wastewater treatment, Journal of Industrial and Engineering Chemistry, https://doi.org/10.1016/j.jiec.2025.02.012.
[11] Khan, M. M. A., Rafiuddin, & Inamuddin. (2013). Synthesis, physico-chemical characterization, transport phenomena and antibacterial activity of polystyrene based barium phosphate composite membrane. Journal of Industrial and Engineering Chemistry, 19(1). https://doi.org/10.1016/j.jiec.2012.07.013.
[12] Arsalan, M., Khan, M. M. A., & Rafiuddin. (2015). Thermodynamic evaluation and electrochemical parameters of PVC-based ion-exchange nickel tungstate composite membrane and their potential applications. Desalination and Water Treatment, 56(7). https://doi.org/10.1080/19443994.2014.951969.
[13] Huang, T., Yan, M., He, K., Huang, Z., Zeng, G., Chen, A., Peng, M., Li, H., Yuan, L., Chen, G., 2019. Efficient removal of methylene blue from aqueous solutions using magnetic graphene oxide modified zeolite. J. Colloid Interface Sci. 543, 43–51. https://doi.org/10.1016/j.jcis.2019.02.030.
[14] Mahmoodi, N.M., Saffar-Dastgerdi, M.H., 2020. Clean Laccase immobilized nanobiocatalysts (graphene oxide - zeolite nanocomposites): From production to detailed biocatalytic degradation of organic pollutant. Appl. Catal. B Environ. 268, 118443. https://doi.org/10.1016/j.apcatb.2019.118443
[15] Liu, X., Liu, Y., Lu, S., Guo, W., Xi, B., 2018. Performance and mechanism into TiO2/Zeolite composites for sulfadiazine adsorption and photodegradation. Chem. Eng. J. 350, 131–147. https://doi.org/10.1016/j.cej.2018.05.141
[16] Sacco, O., Vaiano, V., Matarangolo, M., 2018. ZnO supported on zeolite pellets as efficient catalytic system for the removal of caffeine by adsorption and photocatalysis. Sep. Purif. Technol. 193, 303–310. https://doi.org/10.1016/j.seppur.2017.10.056
[17] Milojević-Rakić, M., Janošević, A., Krstić, J., Nedić Vasiljević, B., Dondur, V., Ćirić-Marjanović, G., 2013. Polyaniline and its composites with zeolite ZSM-5 for efficient removal of glyphosate from aqueous solution. Microporous Mesoporous Mater. 180, 141–155. https://doi.org/10.1016/j.micromeso.2013.06.025
[18] Senguttuvan, S., Janaki, V., Senthilkumar, P., Kamala-Kannan, S., 2022. Polypyrrole/zeolite composite – A nanoadsorbent for reactive dyes removal from synthetic solution. Chemosphere 287, 132164. https://doi.org/10.1016/j.chemosphere.2021.132164
[19] Kamali, M., Esmaeili, H., Tamjidi, S., 2022. Synthesis of Zeolite Clay/Fe-Al Hydrotalcite Composite as a Reusable Adsorbent for Adsorption/Desorption of Cationic Dyes. Arab. J. Sci. Eng. 47, 6651–6665. https://doi.org/10.1007/s13369-022-06580-4.
[20] Baglio, V., Arico, A.S., Blasi, A. Di, Antonucci, P.L., Nannetti, F., Tricoli, V., Antonucci, V., 2005. Zeolite-based composite membranes for high temperature direct methanol fuel cells. J. Appl. Electrochem. 35, 207–212. https://doi.org/10.1007/s10800-004-6202-z.
[21] Pan, X., Jiao, F., Miao, D., Bao, X., 2021. Oxide–Zeolite-Based Composite Catalyst Concept That Enables Syngas Chemistry beyond Fischer–Tropsch Synthesis. Chem. Rev. 121, 6588–6609. https://doi.org/10.1021/acs.chemrev.0c01012.
[22] Zhao, M., Ma, X., Chen, D., Liao, Y., 2022. Preparation of Honeycomb-Structured Activated Carbon–Zeolite Composites from Modified Fly Ash and the Adsorptive Removal of Pb(II). ACS Omega 7, 9684–9689. https://doi.org/10.1021/acsomega.1c07192.
[23] Klaysom, C., Marschall, R., Wang, L., Ladewig, B.P., Lu, G.Q.M., 2010. Synthesis of composite ion-exchange membranes and their electrochemical properties for desalination applications. J. Mater. Chem. 20, 4669. https://doi.org/10.1039/b925357b
[24] Klaysom, C., Moon, S.-H., Ladewig, B.P., Lu, G.Q.M., Wang, L., 2011. The Influence of Inorganic Filler Particle Size on Composite Ion-Exchange Membranes for Desalination. J. Phys. Chem. C 115, 15124–15132. https://doi.org/10.1021/jp112157z.
[25] Imteyaz, S., Rafiuddin, 2016. Transport studies of ions across polystyrene based composite membrane: Evaluation of fixed charge density using theoretical models. J. Mol. Struct. 1123, 116–123. https://doi.org/10.1016/j.molstruc.2016.06.020
[26] Hou, X., Hu, Y., Hu, X., Jiang, D., 2018. Poly (ether ether ketone) composites reinforced by graphene oxide and silicon dioxide nanoparticles. High Perform. Polym. 30, 406–417. https://doi.org/10.1177/0954008317701549.
[27] Jampilek, J., Kralova, K., 2021. Advances in Drug Delivery Nanosystems Using Graphene-Based Materials and Carbon Nanotubes. Materials (Basel). 14, 1059. https://doi.org/10.3390/ma14051059.
[28] Piaskowski, K., Zarzycki, P.K., 2020. Carbon-Based Nanomaterials as Promising Material for Wastewater Treatment Processes. Int. J. Environ. Res. Public Health 17, 5862. https://doi.org/10.3390/ijerph17165862.
[29] Krissanasaeranee, M., Wongkasemjit, S., Cheetham, A.K., Eder, D., 2010. Complex carbon nanotube-inorganic hybrid materials as next-generation photocatalysts. Chem. Phys. Lett. 496, 133–138. https://doi.org/10.1016/j.cplett.2010.07.043
[30] Zafar, F., Khan, S., Ghosal, A., Azam, M., Sharmin, E., Rizwanul Haq, Q.M., Nishat, N., 2019. Clean synthesis and characterization of green nanostructured polymeric thin films from endogenous Mg (II) ions coordinated methylolated-Cashew nutshell liquid. J. Clean. Prod. 238, 117716. https://doi.org/10.1016/j.jclepro.2019.117716
[31] Zafar, F., Khan, S., Mondal, A.H., Sharmin, E., Rizwanul Haq, Q.M., Nishat, N., 2020. Application of FTIR-ATR spectroscopy to confirm the microwave assisted synthesis and curing of Cashew nut shell liquid derived nanostructured materials. Spectrochim. Acta Part A Mol. Biomol. Spectrosc. 228, 117732. https://doi.org/10.1016/j.saa.2019.117732.
[32] Selim, M.S., Shenashen, M.A., Elmarakbi, A., EL-Saeed, A.M., Selim, M.M., El-Safty, S.A., 2017. Sunflower oil-based hyperbranched alkyd/spherical ZnO nanocomposite modeling for mechanical and anticorrosive applications. RSC Adv. 7, 21796–21808. https://doi.org/10.1039/C7RA01343D
[33] Selim, M.S., Shenashen, M.A., Hashem, A.I., El-Safty, S.A., 2018. Linseed oil-based alkyd/Cu 2 O nanocomposite coatings for surface applications. New J. Chem. 42, 10048–10058. https://doi.org/10.1039/C7NJ03440G.
[34] Jiang, Y.-R., Chou, S.-Y., Chang, J.-L., Huang, S.-T., Lin, H.-P., Chen, C.-C., 2015. Hydrothermal synthesis of bismuth oxybromide–bismuth oxyiodide composites with high visible light photocatalytic performance for the degradation of CV and phenol. RSC Adv. 5, 30851–30860. https://doi.org/10.1039/C5RA01702E
[35] Markovich, T., Andelman, D., & Podgornik, R. (2016). Charged membranes: Poisson–Boltzmann theory, DLVO paradigm and beyond. In R. R. Netz & D. Andelman (Eds.), Electrostatic Properties of Membranes (arXiv preprint No. 1603.09451). arXiv. https://arxiv.org/abs/1603.09451
[36] Jabeen, F., Rafiuddin, 2009. Membrane potential and fixed-charge density across TiPO4–VPO4 composite membranes for uni-univalent electrolyte solution. J. Porous Mater. 16, 257–265. https://doi.org/10.1007/s10934-008-9195-x.
[37] Barragán, V.M., Pérez-Haro, M.J., 2011. Correlations between water uptake and effective fixed charge concentration at high univalent electrolyte concentrations in sulfonated polymer cation-exchange membranes with different morphology. Electrochim. Acta 56, 8630–8637. https://doi.org/10.1016/j.electacta.2011.07.060.
[38] Ahmad, H., Zahid, M., Rehan, Z.A., Rashid, A., Akram, S., Aljohani, M.M.H., Mustafa, S.K., Khalid, T., Abdelsalam, N.R., Ghareeb, R.Y., AL-Harbi, M.S., 2022. Preparation of Polyvinylidene Fluoride Nano-Filtration Membranes Modified with Functionalized Graphene Oxide for Textile Dye Removal. Membranes (Basel). 12, 224. https://doi.org/10.3390/membranes12020224.
[39] Amarnath, N., Appavoo, D., Lochab, B., 2018. Eco-Friendly Halogen-Free Flame Retardant Cardanol Polyphosphazene Polybenzoxazine Networks. ACS Sustain. Chem. Eng. 6, 389–402. https://doi.org/10.1021/acssuschemeng.7b02657.

[40] Loiola, A.R., Andrade, J.C.R.A., Sasaki, J.M., da Silva, L.R.D., 2012. Structural analysis of zeolite NaA synthesized by a cost-effective hydrothermal method using kaolin and its use as water softener. J. Colloid Interface Sci. 367, 34–39. https://doi.org/10.1016/j.jcis.2010.11.026.
[41] Sapawe, N., Jalil, A.A., Triwahyono, S., Shah, M.I.A., Jusoh, R., Salleh, N.F.M., Hameed, B.H., Karim, A.H., 2013. Cost-effective microwave rapid synthesis of zeolite NaA for removal of methylene blue. Chem. Eng. J. 229, 388–398. https://doi.org/10.1016/j.cej.2013.06.005
[42] Dong, F., Li, Z., Huang, H., Yang, F., Zheng, W., Wang, C., 2007. Fabrication of semiconductor nanostructures on the outer surfaces of polyacrylonitrile nanofibers by in-situ electrospinning. Mater. Lett. 61, 2556–2559. https://doi.org/10.1016/j.matlet.2006.09.058
[43] Madhavan, A., Giri, S., & Natarajan, T. S. (2016). Miscibility and specific interactions in polyacrylonitrile/polyvinylidene fluoride blends: A spectroscopic and thermal study. Polymer Bulletin, 73(3), 693–709. https://doi.org/10.1007/s00289-015-1524-4
[44] Tiwari, B.K., Muthukumarappan, K., O' Donnell, C.P., Cullen, P.J., 2008. Modelling colour degradation of orange juice by ozone treatment using response surface methodology. J. Food Eng. 88, 553–560. https://doi.org/10.1016/j.jfoodeng.2008.03.021
[45] Karimi-Shamsabadi, M., Behpour, M., Babaheidari, A.K., Saberi, Z., 2017. Efficiently enhancing photocatalytic activity of NiO-ZnO doped onto nanozeoliteX by synergistic effects of p-n heterojunction, supporting and zeolite nanoparticles in photo-degradation of Eriochrome Black T and Methyl Orange. J. Photochem. Photobiol. A Chem. 346, 133–143. https://doi.org/10.1016/j.jphotochem.2017.05.038.
[46] AlShammari, A., Halim, M.M., Yam, F.K., Al-Hardan, N.H.M., Kaus, N.H.M., Umar, K., Qahtan, T.F., Ibrahim, M.N.M., 2019. The effect of substrate temperatures on the structural and conversion of thin films of reduced graphene oxide. Phys. B Condens. Matter 572, 296–301. https://doi.org/10.1016/j.physb.2019.07.018.
[47] Liu, Q., Yan, X., Li, Y., Liu, X., Zhang, L., Wang, Y. (2019). Understanding the relationship between water content and proton conductivity in perfluorosulfonic acid membranes. Journal of Membrane Science, 582, 86–94, https://doi.org/10.1016/j.memsci.2019.03.013
[48] Zhang, X., Wang, R., Wang, M., Lin, S. (2021). Selective ion transport and separation in reverse osmosis membranes: Effect of ion properties and membrane structure. Desalination, 508, 115037, https://doi.org/10.1016/j.desal.2021.115037
[49] Jabeen, F., Rafiuddin, 2007. Preparation and evaluation of effective fixed charge density of titanium phosphate membranes for uni-univalent electrolytes in aqueous solutions. J. Sol-Gel Sci. Technol. 44, 195–202. https://doi.org/10.1007/s10971-007-1622-y.
[50] Arsalan, M., Imteyaz, S., Zeeshan, M., Rafiuddin, 2016. Synthesis, characterization, and electrochemical observation of PVC-supported strontium tungstate inorganic precipitated composite membrane. Desalin. Water Treat. 57, 15293–15303. https://doi.org/10.1080/19443994.2015.1080191.
[51] Zhang, Y., Fu, Y., Yang, H., & Zhang, R. (2020), Donnan potential and ionic transport in charged nanopores and membranes: Effects of multivalent ions and pH, Journal of Membrane Science, 601, 117906, https://doi.org/10.1016/j.memsci.2020.117906.
[52] Mourad, A.H.I., Al-Ghamdi, S.G., & Khalil, H.A. (2019), Electrochemical characterization of ion exchange membranes: Evaluation of Donnan potential and membrane potential behaviors, Journal of Electroanalytical Chemistry, 843, 67–75, https://doi.org/10.1016/j.jelechem.2019.05.042.
[53] Taky, M., Szymczyk, A., & Ghoufi, A. (2021), Charge regulation and Donnan exclusion in nanofiltration membranes: A molecular dynamics approach, Journal of Membrane Science, 621, 118948, https://doi.org/10.1016/j.memsci.2020.118948.
[45] Arfin, T., Rafiuddin, 2011. An electrochemical and theoretical comparison of ionic transport through a polystyrene-based cobalt arsenate membrane. Electrochim. Acta 56, 7476–7483. https://doi.org/10.1016/j.electacta.2011.06.109.
[55] Yan, H., Yang, M., Tang, B., Fu, Q., Lv, Y., 2019, Enhanced separation performance of composite nanofiltration membranes via the incorporation of dopamine-modified graphene oxide, Journal of Membrane Science, 581, 162–172, https://doi.org/10.1016/j.memsci.2019.03.043.
[56] Zhao, C., Xie, M., Yang, Z., Zheng, W., Wang, H., 2020, Ion selectivity and transport mechanisms in advanced ion exchange membranes: A review, Journal of Membrane Science, 595, 117456, https://doi.org/10.1016/j.memsci.2019.117456.
[57] Imteyaz, S., Rafiuddin, 2016a. Synthesis of Phosphonated Poly(vinyl alcohol)-Based Composite Membrane: Effects of Counter and Co-Ions on Its Electrochemical Properties for Separation Applications. Ind. Eng. Chem. Res. 55, 12655–12666. https://doi.org/10.1021/acs.iecr.6b03387
[58] Geise, G.M., Cassady, H.J., Paul, D.R., Logan, B.E., Hickner, M.A., 2014a. Specific ion effects on membrane potential and the permselectivity of ion exchange membranes. Phys. Chem. Chem. Phys. 16, 21673–21681. https://doi.org/10.1039/C4CP03076A
[59] Geise, G.M., Paul, D.R., Freeman, B.D., 2014b. Fundamental water and salt transport properties of polymeric materials. Prog. Polym. Sci. 39, 1–42. https://doi.org/10.1016/j.progpolymsci.2013.07.001.